On the Choice of Voltage Regulators for Droop-controlled Voltage Source Converters in Microgrids to Ensure Stability

Sandeep Bala
ABB Corporate Research
940 Main Campus Dr
Raleigh, NC 27606, USA
Email: sandeep.bala@ieee.org

Giri Venkataramanan
University of Wisconsin-Madison
1415 Engineering Dr
Madison, WI 53706, USA
Email: giri@engr.wisc.edu

***Abstract*—Microgrids are emerging to be an attractive means to cluster various distributed generation systems with local loads while operating either in a grid-connected mode or in an islanded mode in a semi-autonomous fashion. Voltage source converter (VSC) based distributed generation devices are often an essential component in such microgrids, particularly in interfacing dc energy storage devices. While system level control of VSCs that incorporate frequency and voltage droop have been shown to be essential in ensuring autonomous system operation in a distributed manner, the impact of VSC internal voltage regulator dynamics on system stability has not been definitively established. This paper presents a systematic comparison of voltage regulators using a dynamic phasor based model of an inverter system interfaced to an infinite grid; the model is used to examine system stability boundaries. The impact of various options for realizing VSC voltage regulators in conjuction with varying interconnection system impedance parameters are studied to establish stability boundaries for each case. A dynamic phasor model is used to evaluate operating point stability and the results are verified using computer simulation results.**

***Index Terms*—microgrids, voltage source converters, stability, droop.**

I. Introduction

Electrical power distribution circuits that can operate semi-autonomously from the electric grid as energy islands are receiving considerable interest in the context of microgrids [1]. While microgrids are capable of operating as energy islands, for reliability and/or economic reasons, they invariably exchange power with other circuits, including other microgrids and the main electrical grid. Control features of microgrids that incorporate frequency and voltage droop properties inspired by established generation control approach in the large scale electric grid have come to be accepted in order to provide distributed and autonomous operation of the system without the need for any high speed communications among the various generators. Ensuring the stability of the microgrid becomes a critical issue across various network, power flow, and generator configurations. While stability of grid-forming generation devices [2] using rotating machines with classical speed governers and field regulators are well understood, the dynamics of inverter based grid forming generators and/or storage devices are not well understood. Much of the current literature discusses the impact of generation control, while assuming the inverter's internal voltage regulators to be ideal [3]. Some references [4], [5] do consider details of the voltage regulators, but fail to provide physical insight. It has previously been shown that the impedance of the interconnection to the grid can have an appreciable impact on the system behavior [6]. In this paper, a systematic detailed dynamic phasor model that includes the inverter internal voltage regulator and the generation controller that provide frequency and voltage droop characteristics together is developed to study stability of a simple single machine infinite bus system. It is shown that the interplay between the voltage regulator and the generation controller can have a dramatic impact of system stability.

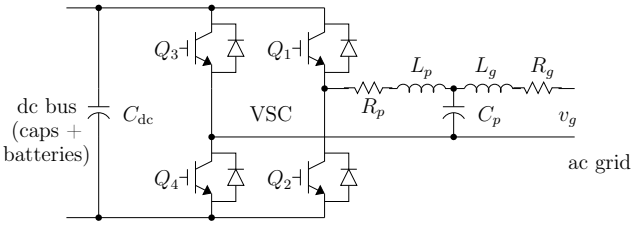

Fig. 1. Power circuit schematic of a single-phase single machine infinite bus (SMIB) system.

Section II describes the physical and control structures of voltage source converters (VSCs) commonly used in microgrids. Section III describes the commonly chosen voltage controllers in such VSCs. Section IV briefly describes the dynamic phasor method used to set up the model of the single machine infinite bus system. Section V shows the results of stability evaluation using the dynamic phasor model and the verification of those results using time-domain simulation models. Finally, section VI lists the conclusions of the study.

II. The voltage source converter in a microgrid

Fig. 1 shows the circuit diagram of a single-phase single machine (the voltage source converter) connected to a voltage source v_g with fixed voltage magnitude and frequency, which

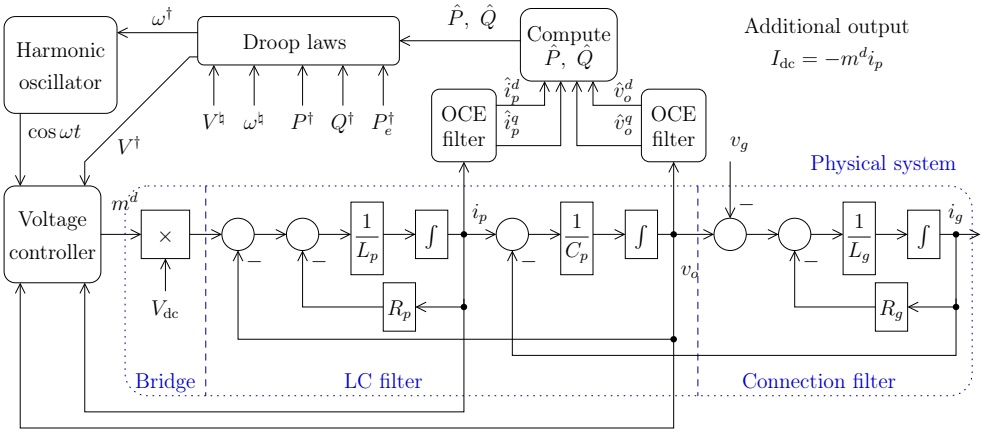

Fig. 2. Overall view of the control structure of a VSC in a microgrid.

models the connection to an infinite bus. Fig. 2 shows the typical control structure of such a single VSC module used in a microgrid. The module's physical system has three sections: the bridge, the LC filter, and the connection filter. The figure depicts the bridge as a perfect average modulator without regard for the switching frequency, because controller design mainly requires low frequency dynamics. But the filter parameters are chosen to filter out the switching frequency component of the output. In the filters, the capacitor is assumed to be ideal, but the inductors are assumed to have a series resistance. The connection filter is modeled as an inductor; if the actual system has an isolation transformer, then the magnetizing reactance can usually be neglected. Table I shows the values of the physical parameters used in this paper. The details of the other blocks illustrated in Fig. 2 are described further.

Although the system under consideration is a single phase system, it is convenient to represent the ac dynamic variables as orthogonal components (in direct and quadrature coordinates) for developing the controls. While orthogonal components in three phase ac systems are readily determined through appropriate transformations, their estimation in single phase systems requires specific signal processing steps. The orthogonal component estimation (OCE) filters of Fig. 3 — elsewhere called SOGI filters [7] — generate the orthogonal component estimates of the output voltage and pole current; the orthogonal components of the ac voltage and current are used to compute the real and reactive power, which are in turn used to generate the frequency and voltage references for the VSC using the droop laws.

$$\hat{P} = \hat{v}_o^d \hat{i}_p^d + \hat{v}_o^q \hat{i}_p^q, \quad \hat{Q} = \hat{v}_o^q \hat{i}_p^d - \hat{v}_o^d \hat{i}_p^d, \tag{1}$$

$$\omega^\dagger = \omega^\natural + b_p(P^\dagger - \hat{P} - P_e^\dagger), \quad \text{and} \tag{2}$$

$$V^\dagger = V^\natural + b_q(Q^\dagger - \hat{Q}). \tag{3}$$

The real and reactive power droop constants b_p and b_q are typically set to about 0.01 pu. $P_e^\dagger$ can be used to influence the power flow in and out of the dc bus; in this paper, this is the control handle used to set the operating point of the VSC.

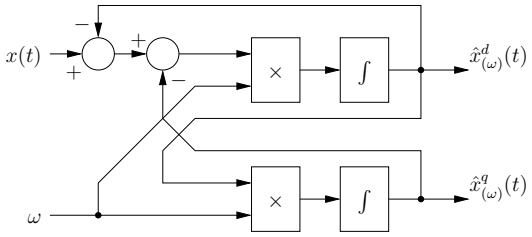

Fig. 3. Orthogonal component estimation (OCE) filter.

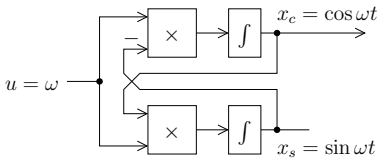

Fig. 4. The harmonic oscillator.

The harmonic oscillator (Fig. 4) generates the sine and cosine values in tune with the frequency reference. The voltage controller block uses the output of the harmonic oscillator together with the voltage magnitude reference to generate the modulation signal m^d of the inverter. Voltage controller options are discussed in detail in the next section.

III. Voltage Controller Options

The voltage controller block of Fig. 2 takes the voltage reference quantities as input and determines the modulation signal to be applied to the VSC modulator. Three classes of voltage controllers are discussed in this section: (A) open loop voltage controllers, which do not use any closed loop feedback for regulation, (B) voltage magnitude controllers, which regulate the voltage magnitude or its square, and (C) voltage waveform controllers, which regulate the waveform of the voltage. The waveform controllers use either (1) a proportional + integral (PI) block or (2) a proportional + resonant (PR) block.

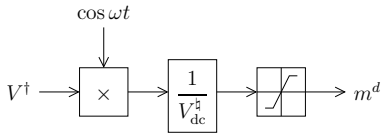

Fig. 5. Block diagram of an open loop voltage controller.

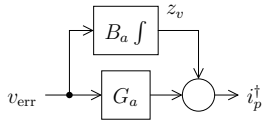

(a) Proportional + Integral (PI) outer voltage controller

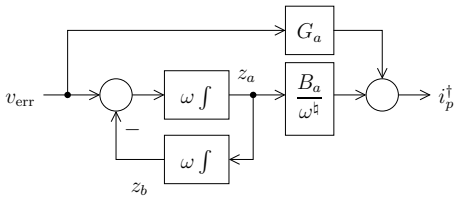

(b) Proportional + Resonant (PR) outer voltage controller

Fig. 8. Block diagrams of the outer loop voltage controller options for voltage waveform control.

A. Open loop control

The open loop voltage controller, shown in Fig. 5, does not use feedback to regulate the output voltage. The voltage waveform reference is divided by the nominal dc bus voltage to obtain the modulation signal. In practice, the microgrid VSC is operated in the linear modulation region by saturating the magnitude of the modulation signal to a value slightly less than unity. A VSC with open loop voltage control typically has poor voltage regulation with respect to changes in the output currents. The poor regulation of the controller of Fig. 5 can be overcome by using feedback to regulate the VSC output voltage as developed in the following subsesctions.

B. Magnitude control

Voltage magnitude controllers attempt to regulate the magnitude, or effectively the rms value, of the output voltage. Two types of magnitude controllers are shown in Fig. 6. The first step in both controllers is to use the orthogonal components of the measured single-phase output voltage to estimate the square of the voltage magnitude. Then, one can choose to regulate either the voltage magnitude, as in Fig. 6(a), or the square of the voltage magnitude, as in Fig. 6(b). A simple PI block serves to regulate the desired quantity. The feed-forward of the nominal voltage magnitude eases the computational burden on the PI controller. The output of the feed-forward summing junction is divided by the nominal voltage magnitude to get the magnitude of the modulation signal. The modulation signal itself is sinusoidal, as long as it is within the saturation bounds.

Regulating the square of the voltage magnitude — henceforth called MSPI control — is nearly equivalent to regulating the magnitude — henceforth called FMPI control; both reach the same steady state, and the dynamics do not differ considerably. FMPI control is computationally more expensive than MSPI control, because it requires a time-intensive square root operation. The MSPI controller is also mathematically more tractable and lends itself to simpler analysis. For these reasons, this paper focuses on MSPI controllers rather than FMPI controllers.

The performance of closed loop magnitude controllers in single-phase systems is limited by the bandwidth of the magnitude estimators. The OCE filters cannot respond quicker than about half the fundamental cycle, so the bandwidth of magnitude controllers can never exceed twice the fundamental frequency.

C. Waveform control

Voltage waveform controllers attempt to regulate the waveform of the output voltage, not just the magnitude. In single-phase systems, they can be tuned to higher bandwidths than magnitude controllers. If the dc bus voltage of the VSC is roughly constant, then the plant is linear, and a linear voltage waveform controller suffices. The general form of such a controller is shown in Fig. 7. The addition of the output voltage at the penultimate stage effectively achieves 'back-emf' decoupling [8]. There is an inner proportional current loop and an outer voltage control loop. The outer voltage controller is commonly either a PI block (Fig. 8(a)) or a PR block (Fig 8(b)).

The PI based voltage waveform controller — henceforth called WFPI controller — results in zero steady state error only at zero frequency; it has a finite steady state error at all other frequencies. This means the WFPI controller rejects all dc disturbances, but has a finite response to ac disturbances.

The PR based voltage waveform controller — henceforth called WFPR controller — is normally tuned so that the resonant frequency is identical to the fundamental frequency. The WFPR controller results in zero steady state error only at the fundamental frequency, and has finite steady state error at other frequencies. This means the WFPR controller rejects all disturbances at the fundamental frequency, but has a finite response to disturbances at dc and non-fundamental ac frequencies. The PR controller is similar to the PI controller, except that the frequency at which it performs best is shifted from dc to the fundamental frequency.

The WFPI and the WFPR controllers are tuned by pole placement. The transfer function of the closed loop can be easily computed and the closed loop eigenvalues placed at desired locations by choosing appropriate gains. Note that the same gains can also be used for the WFPI and WFPR controller, because they are equivalent except for the frequency shift.

D. Notes on hardware implementation

A VSC feeding a variable passive load was set up in the laboratory to verify the performance of different controllers

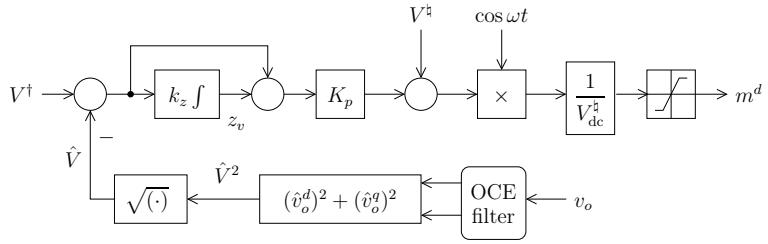

(a) Fundamental magnitude PI (FMPI)

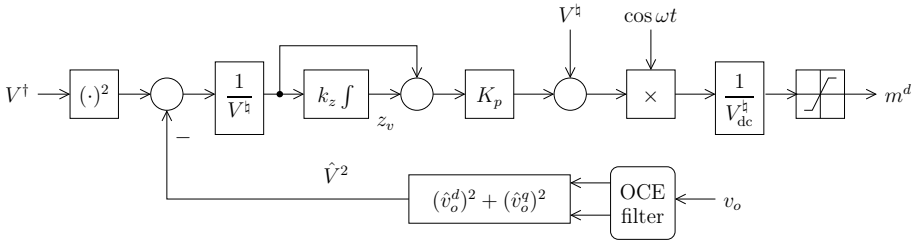

(b) Fundamental magnitude squared PI (MSPI)

Fig. 6. Block diagrams of magnitude PI voltage controllers.

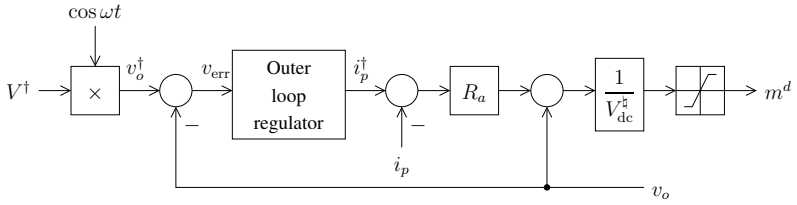

Fig. 7. Complete voltage waveform controller

at 60 Hz output feed a passive load. In tests, the open loop controller had poor regulation, while the MSPI controller was found to regulate the output voltage magnitude of the VSC within acceptable bounds at lower as well as higher fundamental frequencies. The WFPI controller produced 60 Hz output with a voltage magnitude that had some steady state error, but was still within acceptable bounds. The steady state error could be reduced by increasing the capacitance C_p, but this increased the reactive power supplied by the VSC. The WFPR controller produced a clean fundamental component output with minimal steady state error.

IV. Dynamic phasor model

A. Method

The method of modeling single-phase systems using dynamic phasors is described in some detail in [9] and [10]. The steps are recited here for convenience:

1) Write all dynamic equations in terms of actual variables.
2) Decide on the frequency components to include in all state and input variables. This paper only uses the fundamental component of ac variables and the dc component of dc variables
3) Replace the actual state and input variables by their dynamic phasor representations.

TABLE I
Filter parameters and control gains for magnitude and waveform voltage control methods. Base values: voltage = 50 V; power = 400 W.

Filter parameters		
L_p	275 μH	0.016 pu
R_p	0.1 Ω	0.016 pu
C_p	30 μF	0.071 pu
Droop control gains		
b_p	0.0094 rad/s/W	0.01 pu
b_q	0.0018 V/VAr	0.01 pu
Magnitude control method gains		
K_p	1/16	1/16 pu
k_z	25000/8 sec^{-1}	8.289 pu
Waveform control method gains		
$\lambda_{\rm PI}$	$\frac{0.4}{\sqrt{L_pC_p}}, \frac{0.3(1 \pm j2)}{\sqrt{L_pC_p}}$	
R_a	3.028 Ω	0.484 pu
B_a	654.55 Ω^{-1}-s^{-1}	10.851 pu
G_a	0.228 Ω^{-1}	1.424 pu

4) Expand the equations and equate the amplitudes of the sines and cosines of each frequency. This step is justified by the slowly-varying and uncorrelated frequencies assumptions.
5) Solve for the derivatives of the dynamic phasor states.

TABLE II
STATES AND INPUTS IN AN SMIB SYSTEM.

Block	Physical variables	Frequency components	No. of dyn. phasor states
Physical system			
Bridge	-	-	-
LC filter	i_p, v_o	ω	4
Connection filter	i_g	ω	2
Controller system: reference generation			
OCE filter	$\hat{i}_p^d$, $\hat{i}_p^q$, $\hat{v}_p^d$, $\hat{v}_p^q$	ω	8
Compute $\hat{P}$, $\hat{Q}$	-	-	-
Droop laws	-	-	-
Harmonic Oscillator	$\cos\omega t$, $\sin\omega t$	ω	4
Controller system: voltage controller			
Open	-	-	-
MSPI	z_v	0	1
WFPI	z_v	ω	2
WFPR	z_a, z_b	ω	4
Inputs			
Grid	v_g	ω	2
Dc bus	V_{dc}	0	1
External power ref.	$P_e^\dagger$	0	1

After following these steps, one should obtain the dynamic state equations in terms of the dynamic phasor variables. Due to lack of space, the details are omitted here.

B. Model of SMIB system

Table II shows the chosen states and inputs of the SMIB system. The number of states varies according to the type of voltage controller. The length n of the state vector $\mathbf{x}$ ranges from 18 in the case of open loop voltage control to 22 in the case of waveform PR control. The input vector $\mathbf{u}$ has 4 variables. The state equations can be written as n nonlinear dynamic equations $\dot{\mathbf{x}} = f(\mathbf{x}, \mathbf{u})$.

The operating point is fixed by setting known states, setting inputs, and applying additional constraints. Of the n equations, two are redundant because of the nature of dynamic phasor modeling. The zero angle is aligned with the $\cos\omega t$ state, and the state equations describing the dynamics of the $\cos\omega t$ state are discarded. Additionally, the input V_{dc} is set to a fixed value of 2 pu and the input $P_e^\dagger$ is set to a nominal fixed value of 0 pu. Since ω is also an unknown variable, there are in all $n-2$ equations and $n+1$ variables. The difference in the number of equations and unknowns is made up by imposing the following constraints and set points.

- ω is the dc component of the frequency reference as computed by (2).
- The dc component of the estimated power flow is set to any desired value.
- The magnitude of the grid voltage v_g is set to a fixed value of 1 pu.

Now the $n+1$ nonlinear equations can be solved for the unknowns after giving reasonable initial guesses. This gives the operating point.

V. SMIB SYSTEM: OPERATING POINT STABILITY

A. Regions of stability

The dynamic phasor model of the system was implemented in Mathematica [11]. The Jacobian was evaluated at various operating points. The eigenvalues of the Jacobian are the small signal eigenvalues of the system about those operating points.

For each power flow point and voltage control option, the parameter space was scanned to search for three types of points:

1) **Meshed, gray region:** Points where there is no reasonable equilibrium within safe physical operating limits, and the nonlinear equation solver cannot find a solution close to a reasonable starting guess; the dynamic phasor model is inadequate to capture all the dynamics, because there are several non-fundamental frequency components.
2) **Solid, green region:** Points where an equilibrium exists and is stable; all the operating point eigenvalues lie in the closed left half s-plane.
3) **Solid, white region:** Points where an equilibrium exists, but is unstable; there is at least one eigenvalue in the open right half s-plane.

Figs. 9(a), 10(a), 11(a), and 12(a)), which show results for inverter mode of operation of a 60 Hz VSC, indicate that the set of allowed values of connection impedances is larger for laxer voltage magnitude regulation methods (like open loop and MSPI) than for more rigid voltage waveform regulation methods (like WFPI and WFPR). Similar results were also observed for rectifier mode of operation (not shown due to lack of space), with the difference that the meshed, gray region was slightly larger, and the solid, green region was slightly smaller.

The following key observations may be made from the figures:

- Under closed loop voltage control, if the X_g and R_g/X_g ratio are too small, the system is unstable.
- If the X_g and R_g/X_g ratio are too large, the system does not have a reasonable operating point.
- There is a clear hierarchy of the sizes of the regions of stability. In descending order of stability region sizes, the voltage control methods are: open loop control, MSPI control, WFPI control, and WFPR control.

Thus, it would appear that the design of the connection filter is important for the successful integration of a VSC-interfaced grid-forming source into a stiff microgrid. The impedance of the connection filter is given by

$$Z_g = X_g\sqrt{1+(R_g/X_g)^2}. \tag{4}$$

An impedance of 0.01–0.2 pu is a reasonable compromise between too low a value and too high a value. These values lie in the stable region of the open and MSPI controllers, but only partly in the stable region of the WFPI controller. Although the WFPR controller gives the best performance when operating as the only power source, it has the poorest stability region when integrated with a stiff microgrid. The choice of the

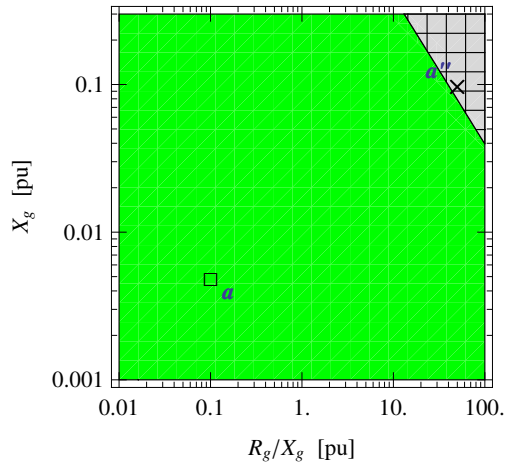

(a) Stability regions for open loop control — Solid/Green: stable; Solid/White: unstable; Meshed/Gray: no steady state within reasonable bounds.

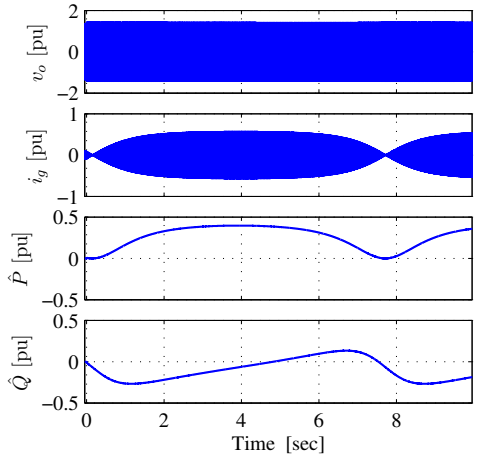

(b) waveforms at unstable point a'' (open)

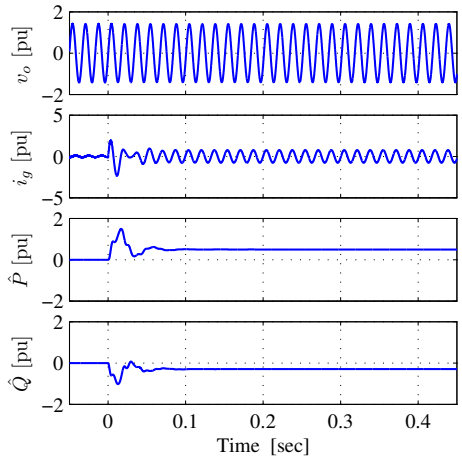

(c) waveforms at stable point a (open)

Fig. 9. Stability regions and waveforms at select points for open loop control of a 60 Hz single-phase microgrid inverter at $+0.5$ pu average output power (inverter mode).

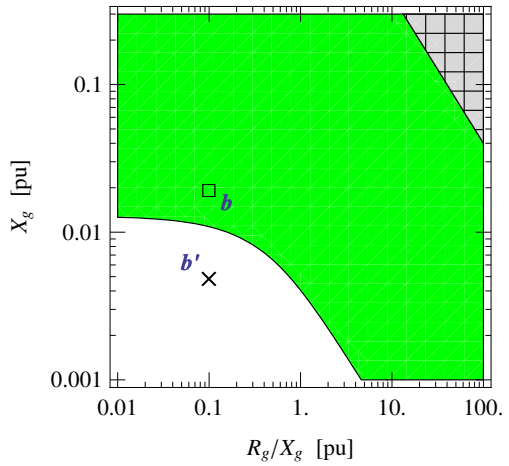

(a) Stability regions for MSPI control — Solid/Green: stable; Solid/White: unstable; Meshed/Gray: no steady state within reasonable bounds.

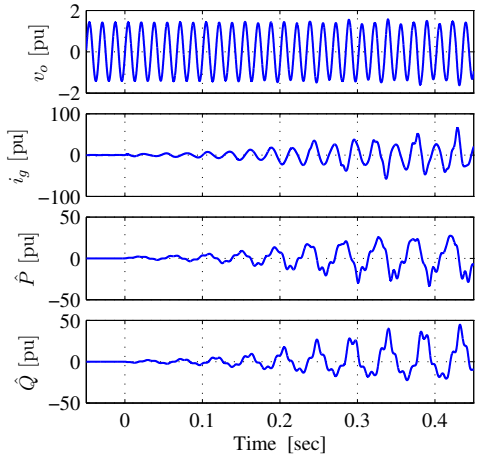

(b) waveforms at unstable point b' (MSPI)

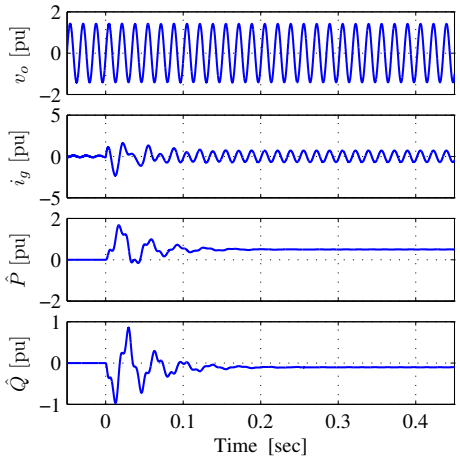

(c) waveforms at stable point b (MSPI)

Fig. 10. Stability regions and waveforms at select points for MSPI control of a 60 Hz single-phase microgrid inverter at $+0.5$ pu average output power (inverter mode).

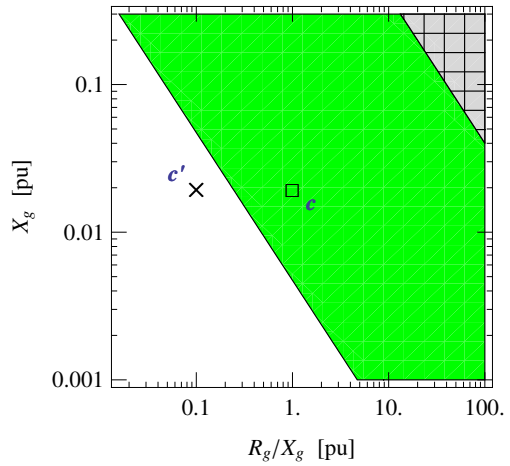

(a) Stability regions for WFPI control — Solid/Green: stable; Solid/White: unstable; Meshed/Gray: no steady state within reasonable bounds.

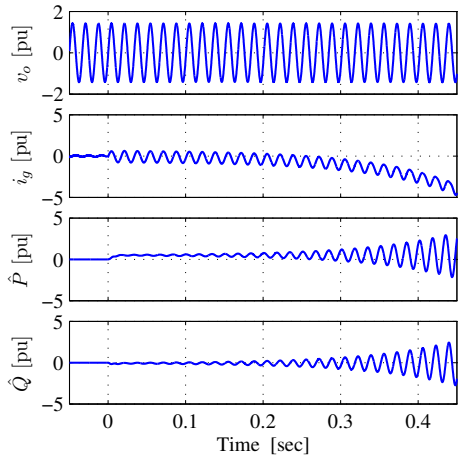

(b) waveforms at unstable point c' (WFPI)

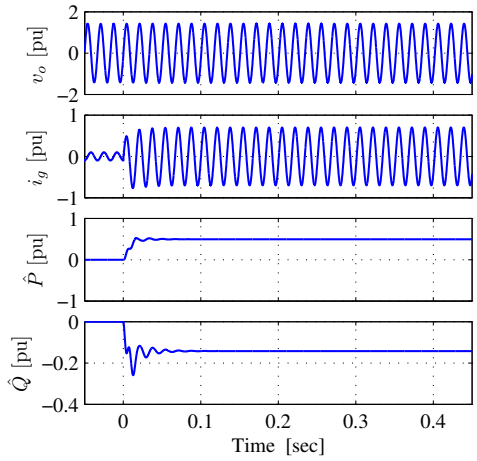

(c) waveforms at stable point c (WFPI)

Fig. 11. Stability regions and waveforms at select points for WFPI control of a 60 Hz single-phase microgrid inverter at $+0.5$ pu average output power (inverter mode).

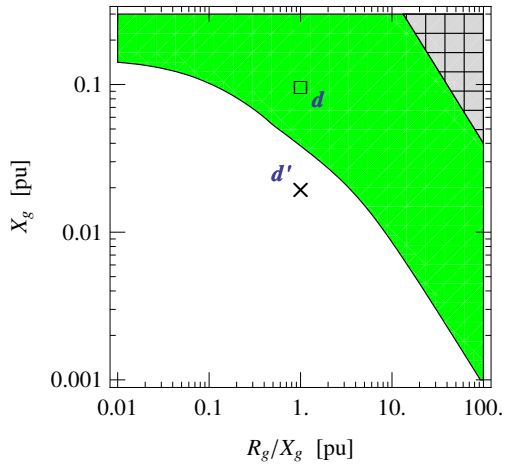

(a) Stability regions for WFPR control — Solid/Green: stable; Solid/White: unstable; Meshed/Gray: no steady state within reasonable bounds.

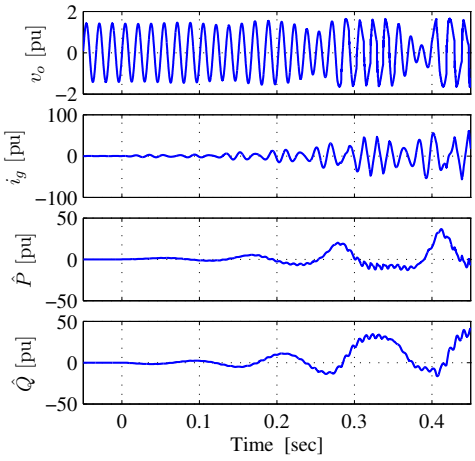

(b) waveforms at unstable point d' (WFPR)

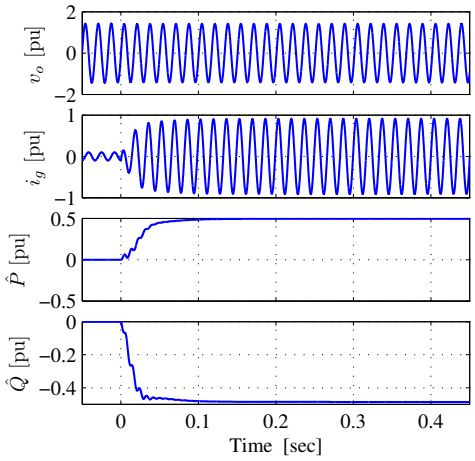

(c) waveforms at stable point d (WFPR)

Fig. 12. Stability regions and waveforms at select points for WFPR control of a 60 Hz single-phase microgrid inverter at $+0.5$ pu average output power (inverter mode).

TABLE III
POINTS AT WHICH SYSTEM WAS SIMULATED. BASE VALUES: VOLTAGE = 50 V; POWER = 400 W.

Point label	R_g		X_g	
a''	5 pu	31.25Ω	0.1 pu	0.625 Ω
$a = b'$	0.0005 pu	0.0031 Ω	0.005 pu	0.0313 Ω
$b = c'$	0.002 pu	0.0125 Ω	0.02 pu	0.125 Ω
$c = d'$	0.02 pu	0.125 Ω	0.02 pu	0.125 Ω
d	0.1 pu	0.625 Ω	0.1 pu	0.625 Ω

voltage control method must be made in conjunction with the connection filter design.

B. Verification via simulations

The above results were also verified via Matlab/Simulink simulations. For each control method, one pathological case and one healthy case were simulated. Table III shows the parameters at the simulation points. The time domain waveforms show that point a'' (Fig. 9(b)) is unstable and point a (Fig. 9(c)) is stable. Point a'' has admittedly unrealistic parameters and was chosen merely to show the behavior of the system at a point in the meshed, gray region. If MSPI control is used at point b' (same as point a), the system is unstable (Fig. 10(b)). The MSPI control could operate stably when the line reactance was increased to that at point b (Fig. 10(c)). But at point c' (same as point b), WFPI control is not stable (Fig. 11(b)); WFPI control becomes stable upon increasing the resistance to point c (Fig. 11(c)). But at point d' (same as point c), WFPR control is unstable (Fig. 12(b)). Increasing the line reactance to that at point d enabled stable operation, as shown in Fig. 12(c).

A final observation in all the waveforms is that if a voltage waveform control method is stable, it has a much better dynamic performance than a voltage magnitude control method. This is reasonable, because waveform control methods have a higher bandwidth.

VI. CONCLUSIONS

The design of a single-phase microgrid VSC module involves the selection of passive component parameters, the selection of the droop constants, and the selection and tuning of a suitable voltage controller. Of these, the droop constants are usually selected based on the power rating of the module. Ordinary inverter design rules can be applied to select the LC filter parameters.

The resistance and reactance of the connection filter along with the voltage control method have a significant impact on the stability of the single machine infinite bus system. Based on the results of the studies presented here, the following recommendations may be made for the design of single-phase microgrid VSC modules.

- The impedance of the connection filter must be low, but not too low. Impedance values of 0.01–0.2 pu are good candidates for evaluation. Too small or too large impedances result in unstable or unsafe operation. If the R_g/X_g ratio is large (> 1), as is common in low voltage wiring, X_g must be small for stable operation; and if the R_g/X_g ratio is small < 1, as is common in higher voltage circuits, then X_g must be large for stable operation.
- Magnitude control methods are better than waveform control methods for stability. The open loop controller is the most robust with respect to stability, the WFPR controller the least. Both these controllers are best avoided; the MSPI and WFPI controllers should be considered.
- The MSPI controller regulates the voltage magnitude to zero steady state error; it works well at low as well as high fundamental frequencies. The WFPI controller results in zero steady state error only at zero frequency; the error increases with frequency; so the WFPI controller is best used only at lower fundamental frequencies.
- Waveform control methods, when stable, are better than magnitude control methods for transient behaviour. So, if both the MSPI and the WFPI are otherwise acceptable, the WFPI controller should be preferred.

ACKNOWLEDGMENTS

The authors gratefully acknowledge the financial sponsorship of this work by the Wisconsin Electric Machines and Power Electronics Consortium (WEMPEC). This work was supported in part by grant number 02524744 "System Integration of Distributed Generation" from the National Science Foundation to the University of Wisconsin-Madison. This work also used shared facilities provided by the ERC program of the National Science Foundation to the Center for Power Electronics Systems (CPES) at the University of Wisconsin-Madison under award number EEC-9731677.

REFERENCES

[1] J. Driesen and F. Katiraei, "Design for distributed energy resources," *IEEE Power and Energy Magazine*, vol. 6, pp. 30–40, May/June 2008.

[2] J. Sachau and A. Engler, "Static and rotating grid formation for modularly expandable island grids," in *Proceedings of 8th European Conference on Power Electronics and Applications. EPE 99*, (Lausanne, Switzerland), 1999.

[3] G. Venkataramanan and M. Illindala, "Small signal dynamics of inverter interfaced distributed generation in a chain-microgrid," in *IEEE PES General Meeting*, 2007.

[4] N. Pogaku, M. Prodanovic, and T. C. Green, "Modeling, analysis and testing of autonomous operation of an inverter-based microgrid," *IEEE Transactions on Power Electronics*, vol. 22, pp. 613–625, Mar. 2007.

[5] I.-Y. Chung, W. Liu, D. A. Cartes, E. G. Collins, and S.-I. Moon, "Control methods of inverter-interfaced distributed generators in a microgrid system," *IEEE Transactions on Industry Applications*, vol. 46, pp. 1078–1088, May 2010.

[6] M. Liserre, R. Teodorescu, and F. Blaabjerg, "Stability of grid-connected PV inverters with large grid impedance variation," in *IEEE PESC*, pp. 4773–4779, 2004.

[7] M. Ciobotaru, R. Teodorescu, and F. Blaabjerg, "A new single-phase PLL structure based on second order generalized integrator," in *Power Electronics Specialists Conference, 2006. PESC '06. 37th IEEE*, pp. 1–6, June 2006.

[8] M. J. Ryan, W. E. Brumsickle, and R. D. Lorenz, "Control topology options for single-phase UPS inverters," *IEEE Transactions on Industry Applications*, vol. 33, pp. 493–500, Mar. 1997.

[9] A. M. Stankovic, S. R. Sanders, and T. Aydin, "Dynamic phasors in modeling and analysis of unbalanced polyphase AC machines," *IEEE Transactions on Energy Conversion*, pp. 107–113, Mar. 2002.

[10] S. Bala, *Integration of Single-phase Microgrids*. PhD thesis, University of Wisconsin-Madison, 2008.

[11] "Wolfram Mathematica 7 Documentation." Available online: http://reference.wolfram.com.